HRTEM and Micro-Raman Studies on Superconducting−Superionic Conducting Nanohybrid, $Ag_{1.17}I_{1.54}Bi_2Sr_2CaCu_2O_y$

Jin-Ho Choy,* Young-Il Kim, Seong-Ju Hwang, Yuji Muraoka,† Naoyuki Ohnishi,† Kenji Hiraga,† and Pham V. Huong‡

National Nanohybrid Materials Laboratory, School of Chemistry and Molecular Engineering, Seoul National University, Seoul 151-747, Korea, Institute for Materials Research, Tohoku University, Katahira, Aoba-ku, Sendai 980-77, Japan, and Laboratoire de Physico-Chimie Moléculaire, Université Bordeaux I, 351, Cours de la Libération, 33405 Talence, France

Received: September 1, 1999

The crystal structure of the superconducting−superionic conducting nanohybrid, $Ag_{1.17}I_{1.54}Bi_2Sr_2CaCu_2O_y$, has been investigated by performing high-resolution transmission electron microscopy (HRTEM) and micro-Raman spectroscopy. From the HRTEM image along the [110] direction, it is found that a hexagonal-like array of AgI_4 tetrahedra is stabilized between each $[Bi-O]_2$ double layer with a staggered configuration of host block. The two-dimensionally extended Ag−I sublattice provides a favorable migration path for Ag^+ ions that is consistent with high ionic conductivity of the Ag−I intercalate. According to the polarized micro-Raman spectroscopy, the doubly split O_{Sr} phonon line is collapsed into a single one upon Ag−I intercalation, as observed in the phase of $IBi_2Sr_2CaCu_2O_y$. Such an evolution of the O_{Sr} phonon peak is surely attributed to a weakening of the $O_{Bi}-Bi-O_{Sr}$ coupling due to the remarkable lattice expansion, which is in good agreement with the HRTEM result.

Introduction

In recent years, the intercalation into Bi-based cuprates has been studied extensively, not only to investigate the mechanism responsible for high-T_c superconductivity of layered oxides, but also to develop new chemical ways of fabricating high-T_c superconducting nanoparticles or thin films.[1−3] Such research efforts have led to the synthesis of various intercalation compounds with artificially controlled crystal structure or electronic configuration. Whereas most of the work in this area has focused mainly on the evolution of the superconductivity of the host lattice,[1] our previous studies revealed that some unusual and exciting physicochemical properties can be derived by hybridizing guest species with a superconducting host lattice.[2,4] For example, a novel mixed ionic−electronic conductivity was accomplished in the $Ag_xI_wBi_2Sr_2Ca_{n-1}Cu_nO_y$ ($0.75 \le x \le 1.2$; $n = 1$, 2, and 3) system where the existence of interstratified structures between the ionic conducting Ag−I layer and the electronic conducting oxide one has been proposed.[4] Surprisingly, the Ag−I intercalates show fast Ag^+ ionic conductivity ($10^{-4}-10^{-1}$ Ω^{-1} cm^{-1}) in a temperature range of 25−270 °C, though their conduction networks are spatially limited to two dimensions because of the layer structure of the host lattice. To understand the occurrence of such a high ionic conductivity for these silver iodide derivatives, their crystal structures should be exactly elucidated because the ionic transport in a solid is essentially structure dependent.[5] However, a conventional characterization method like powder X-ray diffraction (XRD) could not probe directly the intracrystalline Ag−I structure because of the extreme structural anisotropy of the intercalate. In an attempt to find an alternative method, we previously performed X-ray absorption spectroscopy (XAS) for $Ag_xI_wBi_2Sr_2Ca_{n-1}Cu_nO_y$ ($n = 1$, 2, and 3) and found that the intercalated Ag^+ ions are stabilized in the tetrahedral sites with neighboring four iodide ligands.[4c] Although such an XAS analysis is effective in determining the local structure of the intercalated Ag and I, it does not furnish complete structural information on the two-dimensional Ag−I sublattice. To overcome this limitation, high-resolution transmission electron microscopy (HRTEM) is used to visualize the internal atomic arrangement with almost atomic resolution, as in the case of iodine intercalate.[6]

In this paper, we report on the HRTEM images of $Ag_{1.17}I_{1.54}Bi_2Sr_2CaCu_2O_y$ (AgIBi2212) along the *c*-axis, with the aid of a one-dimensional Fourier electron density calculation and extended X-ray absorption fine structure (EXAFS) analysis. In addition, micro-Raman spectroscopy has been carried out to probe the chemical bonding nature of intercalated silver iodide and also the evolution of the electronic and crystal structures of the host lattice upon intercalation. Micro-Raman spectroscopy is quite sensitive to structural distortion around Ag^+ ions in AgI-related compounds,[7−9] and moreover the small area of an Ar^+ laser beam allows us to obtain the polarized Raman spectra with different scattering geometries even for polycrystalline Ag−I intercalation compounds. In particular, it is shown that the *zz*-polarized Raman spectrum provides important information on the effect of intercalation on the host lattice.[10−12]

Experimental Section

Sample Preparation and Characterization. The pristine $Bi_2Sr_2CaCu_2O_y$ (Bi2212) was prepared by conventional solid-state reaction, whereas its Ag−I intercalate was synthesized by heating the homogeneous mixture of the pristine polycrystal with silver metal powder in an I_2 atmosphere [$P(I_2) \cong 1$ atm] at 170 °C for 3 h, and then in air at 190 °C for 10 h.[4,13] The formation

* To whom all correspondence should be addressed. Tel. (82) 2-880-6658; fax (82) 2-872-9864; e-mail jhchoy@plaza.snu.ac.kr.
† Tohoku University.
‡ Université Bordeaux.

10.1021/jp993096w CCC: $19.00
Published on Web 09/13/2000

of single phasic Ag−I intercalate was confirmed by powder XRD measurement using Ni-filtered Cu Kα radiation with a graphite diffracted beam monochromator. A slight T_c depression of 13 K upon intercalation was measured by performing direct-current magnetic susceptibility measurements with a SQUID magnetometer. The chemical composition was determined to be $Ag_{1.17}I_{1.54}Bi_2Sr_2CaCu_2O_y$ by electron microprobe analysis.

TEM Measurement. The HRTEM image was obtained using a 400-kV electron microscope JEM-4000EX with a theoretical resolution of 1.7 Å. The specimen for HRTEM observation was prepared by performing ion milling at 77 K with Ar^+ ion acceleration at 2 kV and an incident angle of 10°.

Micro-Raman Measurement. The micro-Raman spectra presented here were recorded on a Dilor-Omars microspectrometer coupled with an optical microscope (spatial resolution of 1 μm^2) and an intensified 1024-channel photodiode array detector. The 514.5-nm line from an argon ion laser Spectra Physics model 2016 was used as an excitation source. All the present spectra were measured by backscattering from freshly fractured surfaces of the pellet. The polarized Raman spectra with different scattering geometries could be obtained for the polycrystalline AgIBi2212 sample by focusing the Ar^+ laser beam with a diameter of 1 μm on various grains with dissimilar orientations. Under the optical microscope, a vertically aligned grain looks like a narrow rectangular bar, which can be discriminated from the platelike morphology of a parallel-aligned grain. To minimize damage to the sample by the photodissociation effect, the power of the incident laser light was maintained below 0.1 W. The resolution of the present spectra was 3−4 cm^{-1}.

Results and Discussion

Electron Diffraction Pattern. The electron diffraction patterns of AgIBi2212, taken with the incident electron beam parallel to the [001], [010], and [110] directions, are shown in Figure 1. The basal spacing is determined to be ∼14.8 Å, indicating the formation of the first staged AgI intercalate. The lattice expansion of ∼7.4 Å is approximately twice the van der Waals diameter of an iodine atom (∼3.7 Å), implying that the iodine double layers are stabilized in between the $[Bi-O]_2$ slab. Diffuse streaks along the *c*-axis are observed in Figure 1c, indicating the presence of partial inhomogeneous stacking. On the other hand, the in-plane *a* and *b* lattice parameters are found to remain nearly the same as those of the pristine compound, suggestive of little effect of intercalation on the host block.

HRTEM Image. Figure 2 represents the phase-contrast electron micrograph of AgIBi2212 viewed from the [110] direction, where the dark image accounts for the electron density or the atomic distribution. We can discern the dominant horizontal pattern reflecting structural anisotropy of AgIBi2212, together with the well-developed 1:1 interstratification between the Bi2212 sheet and Ag−I sublattice in between every $[Bi-O]_2$ slab, the intercalated Ag−I lattice is identified by twin parallel rows, which would originate from the double layers of iodine. However, no dark spots corresponding to silver ions can be detected even though the atomic scattering factor of silver is comparable with that of iodine.[14] To explain such unexpected HRTEM results, we assumed two kinds of structural models for AgIBi2212 by taking into account the bonding geometry around Ag^+ and the volume demand for the intercalated Ag−I sublattice. According to the previous EXAFS analysis for the Ag−I intercalate, it was found that a silver ion bonds to four iodides at the tetrahedral apexes, whereas an iodide ion is coordinated with only three silver ions. This indicates that the

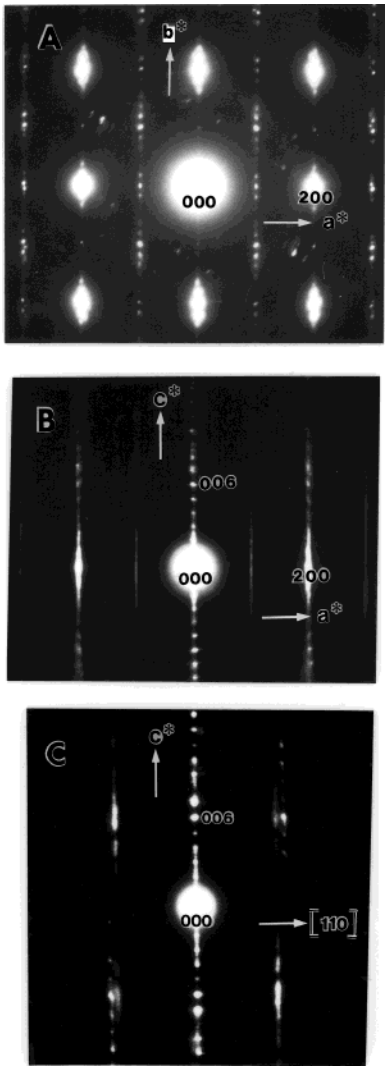

Figure 1. Electron diffraction patterns for AgIBi2212, taken from the (a) [001], (b) [010], and (c) [110] directions.

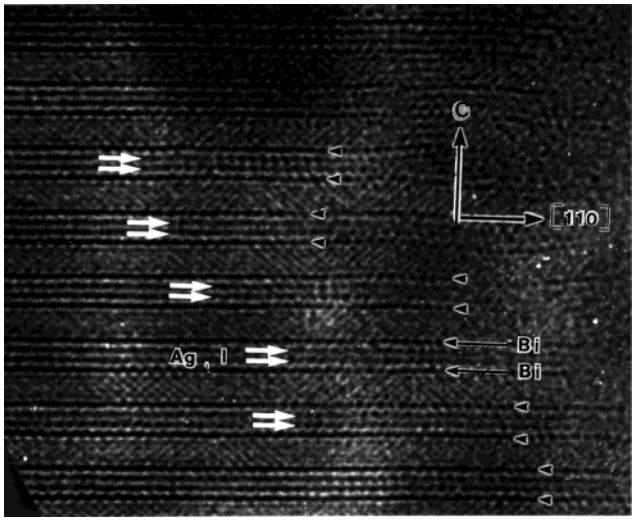

Figure 2. Phase-contrast HRTEM image for AgIBi2212, viewed along the crystal [110] direction.

interlayer Ag−I sublattice is composed of AgI_4 tetrahedra interconnected to form a two-dimensional lattice,[4a] where the iodides are not fully coordinated with silver and are surfaced with the Bi−O plane of the host lattice. Considering that the gallery height of the Ag−I intercalate ($\Delta d \cong 7.4$ Å) is twice

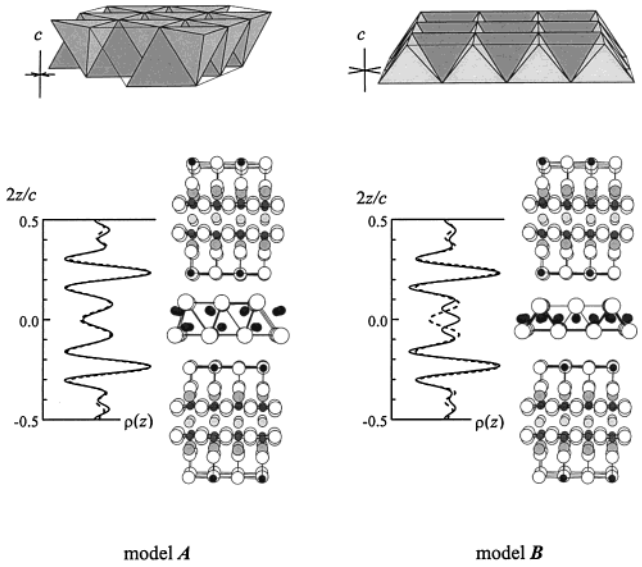

Figure 3. Proposed model structures for the interlayer iodide lattice of AgIBi2212, together with the corresponding Fourier electron density along the *c*-axis. For the Fourier electron density, the calculated data (thick lines) are compared with the experimental data (thin lines).

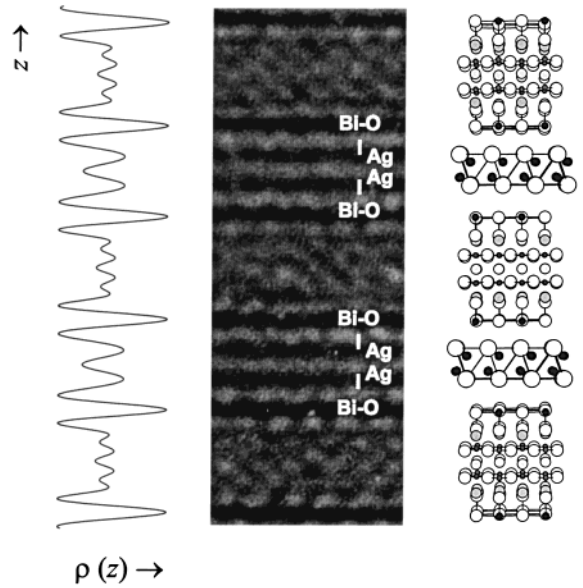

Figure 4. The *c*-axial electron density and the HRTEM image for AgIBi2212, together with the crystal structure model.

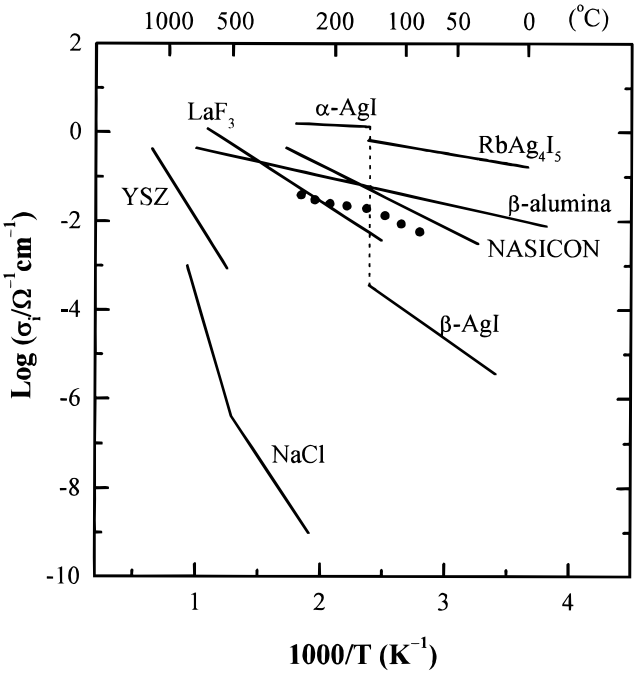

Figure 5. Ionic conductivity of AgIBi2212 (shown as the solid circles), compared with the previously published data for the well-known solid ionic conductors AgI,[16] $RbAg_4I_5$,[17] Na^+-β-alumina,[18] YSZ,[19] NASICON,[20] LaF_3, and NaCl.[21]

that of iodine intercalate, it is reasonably expected that the AgI_4 tetrahedra should be arranged in a monolayer. For further structural description of the interlayer Ag−I lattice, it was necessary to determine the connection pattern and the orientation of the AgI_4 tetrahedra. The AgI_4 tetrahedra can be interconnected in various ways, creating numerous different structures, but it can be readily recognized that only two lattice types are compatible in the present case. To construct an infinite two-dimensional Ag−I lattice with a limitation to the *c*-axial space, each AgI_4 tetrahedron should be arranged as illustrated in Figure 3, where one face (model *A*) or two edges (model *B*) are parallel to the *ab* plane. To evaluate these structural models, one-dimensional electron density maps along the *c*-axis are calculated in the following two ways:[2,14,15] First, the *c*-axial electron density profiles [$\rho(z)$] of AgIBi2212 can be obtained from the summation $\Sigma_{00l}[F_{00l}\cos(2\pi lz)]$ using structure factors determined from X-ray (*00l*) diffraction intensities. The magnitude of the structure factor, $|F_{00l}|$, is the square root of the corrected intensity, I_{00l}/L_p, where I_{00l} and L_p correspond to the observed intensity and the Lorentz polarization factor at a specific diffraction angle, respectively. Because the signs of the F_{00l}s are subject mainly to the *z*-coordinates of heavy ions in the Bi2212 lattice, the phase problem could be solved by assuming conservation of the internal structure of host blocks during the intercalation. Alternatively, F_{00l}s and $\rho(z)$ could be calculated theoretically for a given intracrystalline structure of Ag−I sublattice in AgIBi2212. The one-dimensional electron density maps simulated on the basis of the structure models *A* and *B* are compared in Figure 3 with that obtained from the experimental XRD data. As expected from the different layer stacking sequences of ···/BiO/I/Ag/Ag/I/BiO/··· (model *A*) and ···/BiO/I/Ag/I/BiO/··· (model *B*), the simulated patterns are clearly distinguished at the guest layer region. Between them, the calculated $\rho(z)$ profile with model *A* agrees well with the experimental one, ensuring the fitness of this model. Both in the $\rho(z)$s based on the XRD and on model *A*, each of the peaks centered at $2z/c = \pm 0.08$ is attributed to the presence of Ag and I. Because both ions are located on *c*-axially adjacent layers, their individual contributions are not separated but observed as a single component. Such a result provides an explicit explanation of the double-layered HRTEM pattern of the interlayer Ag−I lattice. For the sake of clear illustration, a magnified HRTEM image is presented in Figure 4, together with the $\rho(z)$ profile calculated from the structure model *A*, demonstrating a good coincidence between the dark spots in the electron microscope image and the peaks in the electron density map.

The above interpretation of the HRTEM image allows us to understand the excellent ionic conductivity of AgIBi2212 as high as $10^{-2}-10^{-1}\ \Omega^{-1}\ cm^{-1}$ in the range 80−270 °C. In Figure 5, the ionic conductivity of AgIBi2212 is compared with those of several ionic solids including representative superionic conductors[5] α-AgI, $RbAg_4I_5$, β-alumina ($NaAl_{11}O_{17}$), NASICON ($Na_{1+x}Zr_2P_{3-x}SiO_xO_{12}$, $0 \le x \le 3$), and YSZ ($ZrO_2-8\%\ Y_2O_3$). As can be well recognized from the plot, AgIBi2212 shows an ionic conductivity comparable with those of the superionic

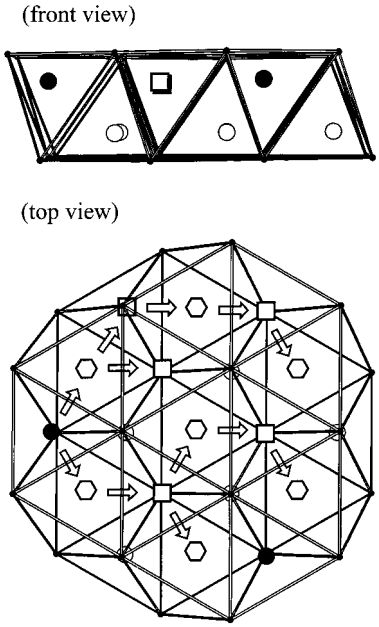

Figure 6. Framework of Ag−I sublattice in AgIBi2212, where Ag^+ (filled or open circles) and I^- (dots) ions are represented together with the available T_d (squares) and O_h (hexagons) sites for Ag^+. Most probable migration path of Ag^+ ion includes the interconnection between the alternating T_d and O_h sites.

conductors. In general, typical superionic conductivity is from the characteristic crystal structure favoring the migration of mobile ionic species and providing a large number of vacant sites with similar lattice energies and a low activation barrier. Upon intercalation of Ag^+ ions into $IBi_2Sr_2CaCu_2O_y$, the iodide lattice is rearranged to provide diffusion paths for the Ag^+ ions in such a way that high ionic conductivity could be realized in AgIBi2212. As shown in Figure 6, there are two-dimensional channels for the Ag^+ ion transport, where each I_4 tetrahedron shares its faces with three neighboring I_6 octahedra, and its edges with four I_4 tetrahedra. This hexagonal-like array of AgI_4 tetrahedra would play a role as an effective passageway for Ag^+ ion transport. In such an intracrystalline structure of the interlayer silver iodide, the Ag^+ ion in a tetrahedral site (T_d) can move into an adjacent tetrahedral (T_d') or an octahedral one (O_h), passing through the edge or face of the AgI_4 tetrahedron, respectively, under an electric field. Because the intermediate state of the linear AgI_2 state ($R_{Ag-I} \cong 2.3$ Å) for the $T_d \rightarrow T_d'$ migration is expected to be less stable than the trigonal AgI_3 state ($R_{Ag-I} \cong 2.65$ Å) for the $T_d \rightarrow O_h$ one,[22] it can be concluded that the Ag^+ ion is transported along the conduction path ...$-T_d-O_h-T_d-O_h-T_d-$....

From a closer examination on the HRTEM image, we found that the Ag−I intercalate retains the staggered configuration of a host block that is characteristic of the pristine compound,[23] as shown in Figure 7. This is surely in contrast to the iodine intercalate, whose host block is translated by $(a + b)/2$ upon intercalation, resulting in a straight aligned configuration of the host lattice.[1] Such different effects of iodine and silver iodide intercalation on the crystal structure of Bi2212 can be explained from the distinct symmetry of the guest layer, which means that a mirror plane does not exist in the intercalated Ag−I layer for AgIBi2212, unlike IBi2212.[24] On the basis of the fact that the intercalation of silver iodide is achieved in two steps: (a) iodine intercalation and (b) Ag^+ diffusion into the preintercalated iodine sublattice,[4] the crystal structure of Bi2212 is considered to change twice during AgI intercalation, namely, from a staggered configuration to a straight aligned configuration in

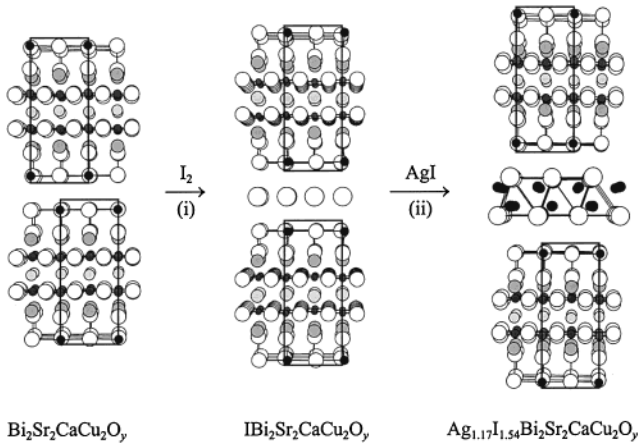

Figure 7. Structural evolution of host lattice upon (i) iodine and (ii) silver iodide intercalation.

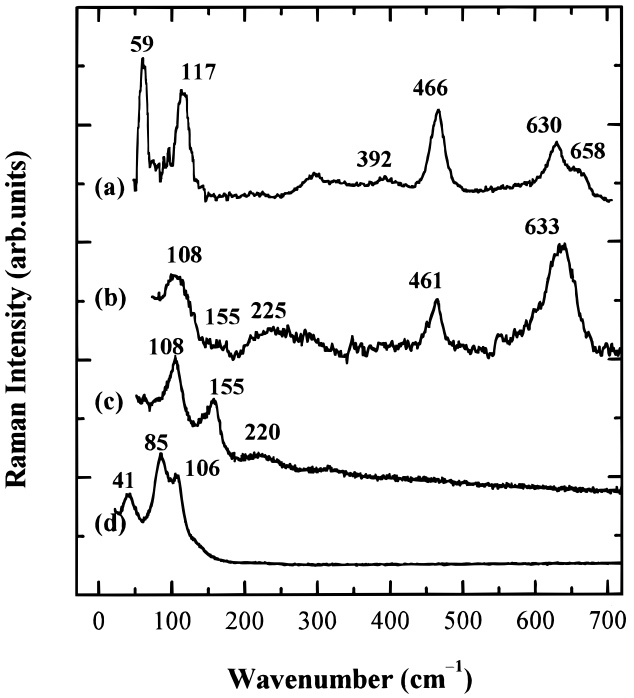

Figure 8. Micro-Raman spectra of (a) Bi2212 and of AgIBi2212 with (b) *c*-axis and (c) *ab*-plane polarization, in comparison with (d) the reference β-AgI.

the first step and then back to a staggered configuration in the second step, as illustrated in Figure 7. This implies that the host block can glide easily to stabilize the overall crystal lattice even at temperature below 200 °C.

Micro-Raman Analysis. The effect of silver iodide intercalation on the chemical bonding environment of the host lattice has also been examined by performing micro-Raman measurements. Figure 8 shows the micro-Raman spectra of the pristine Bi2212 and its silver iodide intercalate, and that of β-AgI as a reference for comparison. On the basis of previous polarization experiments for the pristine compound,[25,26] two strong peaks at 59 and 117 cm^{-1} are assigned as the *c*-axis vibrations of Bi and Sr, respectively, whereas the higher-frequency phonon lines at 466 and 630/658 cm^{-1} are interpreted as the A_{1g} modes of O_{Bi} and O_{Sr}, respectively. Among them, the phonon line at 466 cm^{-1} is expected to serve as a sensitive probe to the variation of the Bi−O layer, which is known to be severely affected by the intercalation reaction.[27] Other weak peaks are also observed at 140 and 392 cm^{-1}, which are ascribed to the A_{1g} vibrations

of Cu and O_{Cu}, respectively.[25] In addition, there is a broad spectral feature around 300 cm^{-1} corresponding to the overlap of the B_{1g} vibration of O_{Cu} and the tetragonal forbidden modes of O_{Bi}/O_{Sr}.[25,28]

For the Ag−I intercalate, two different spectra were available, as shown in Figure 8b and c, depending on the way of focusing the laser beam on various grains with dissimilar orientations. Because the peak at 633 cm^{-1} corresponding to the A_{1g} vibration of O_{Sr} is exclusively detected for *zz* scattering geometry, the spectrum of Figure 8b can be attributed to the *c*-axis polarized data and that of Figure 8c to the *ab*-plane polarized one, respectively. For both scattering geometries, the spectral features from the guest Ag−I layer, which appear in a low-frequency region of <200 cm^{-1}, are quite different from that from the reference β-AgI. According to the previous unpolarized Raman results for this derivative,[4d] the intracrystalline structure of the Ag−I layer was reported to be an α-AgI-type disordered lattice structure. Therefore, the broad peak at $\sim$108 cm^{-1} can be ascribed to $A_1(TO)/E_1(TO)$, whereas the weak shoulders at $\sim$155 and $\sim$220 cm^{-1} are assigned as $A_1(LO)/E_1(LO)$ and the overtone of $A_1(TO)/E_1(TO)$, respectively.[7] In addition to these phonon modes in the low-frequency region, Raman peaks corresponding to oxygen vibrations are also detected at 461 and 633 cm^{-1}, which are attributed to the A_{1g} modes of O_{Bi} and O_{Sr}, respectively.[25,26] As shown in Figure 6a and b, a doubly split feature of the O_{Sr} vibration for the pristine compound is collapsed into a single peak upon Ag−I intercalation. Because this doublet originates from in-phase and out-of-phase O_{Bi} anharmonic motions in $[Bi-O]_2$ bilayers of Bi2212, it can be observed only for the close and staggered configurations of the host lattice.[10,12] Even though the present electron microscopic result indicates that the staggered configuration of the pristine compound remains unchanged after the Ag−I intercalation, a collapse of the O_{Sr} doublet is also detected for the Ag−I intercalate, as in the case of iodine intercalate.[10] Therefore, such a peak collapse can be interpreted as a result of lattice expansion that causes the suppression of $O_{Bi}-Bi-O_{Sr}$ coupling, regardless of the change in configuration of the host block. Actually, this phenomenon has also been observed for other compounds such as iodine, iodobromide, and metal halide intercalates.[10,11,29] Therefore, it is available as an indicator of the intercalation of guest species between $[Bi-O]_2$ double layer of bismuth cuprates.

Conclusion

From the HRTEM and one-dimensional Fourier electron density calculations for AgIBi2212, we were able to verify that an edge-shared array of AgI_4 tetrahedra with α-AgI geometry is stabilized between the $[Bi-O]_2$ double layers of Bi2212 with a staggered configuration of the host block. It is, therefore, not surprising that the Ag^+ ions are fast ionic conducting in the lattice of AgIBi2212, and such a high conductivity can be described by the continuous hopping of Ag^+ through alternating T_d and O_h sites in the two-dimensional Ag−I sublattices. From the micro-Raman study, it is understood that the interlayer Ag−I lattice is formed with substantial disorder, similar to that in the α-AgI phase. As an effect of Ag−I intercalation, the doubly split O_{Sr} phonon line is found to collapse into a single peak. Taking into account the HRTEM observations, we can ascribe this spectral feature to the weakening of interlayer interaction between adjacent Bi−O planes induced by lattice expansion rather than to the change of configuration pattern of the host block.

Acknowledgment. This work was supported in part by the Ministry of Science and Technology through the 1999 National Research Laboratory project and in part by the Ministry of Education through the Brain Korea 21 project.

References and Notes

(1) (a) Xiang, X.-D.; McKernan, S.; Vareka, W. A.; Zettl, A.; Corkill, J. L.; Barbee, T. W., III; Cohen, M. L. *Nature* **1990**, *348*, 145. (b) Choy, J.-H.; Kang, S.-G.; Kim, D.-H.; Hwang, S.-J.; Itoh, M.; Inaguma, Y.; Nakamura, T. *J. Solid State Chem.* **1993**, *102*, 284. (c) Subramanian, M. A. *J. Solid State Chem.* **1994**, *110*, 193.

(2) (a) Choy, J.-H.; Park, N.-G.; Hwang, S.-J.; Kim, D.-H.; Hur, N.-H. *J. Am. Chem. Soc.* **1994**, *116*, 11564. (b) Bae, M.-K.; Kim, M.-S.; Lee, S.-I.; Choy, J.-H.; Park, N.-G.; Hwang, S.-J.; Kim, D.-H. *Phys. Rev. B* **1996**, *53*, 12416. (c) Choy, J.-H.; Park, N.-G.; Hwang, S.-J.; Khim, Z.-G. *J. Phys. Chem.* **1996**, *100*, 3783. (d) Choy, J.-H.; Hwang, S.-J.; Park, N.-G. *J. Am. Chem. Soc.* **1997**, *119*, 1624.

(3) (a) Choy, J.-H.; Kwon, S.-J.; Park, G.-S. *Science* **1998**, *280*, 1589. (b) Choy, J.-H.; Kwon, S.-J.; Hwang, S.-J.; Kim, Y.-I.; Lee, W. *J. Mater. Chem.* **1999**, *9*, 129.

(4) (a) Choy, J.-H.; Park, N.-G.; Kim, Y.-I.; Hwang, S.-H.; Lee, J.-S.; Yoo, H.-I. *J. Phys. Chem.* **1995**, *99*, 7845. (b) Choy, J.-H.; Park, N.-G.; Kim, Y.-I.; Kim, C.-H. *Eur. J. Solid State Inorg. Chem.* **1995**, *t32*, 701. (c) Choy, J.-H.; Kim, Y.-I.; Hwang, S.-J. *J. Phys. Chem. B* **1998**, *102*, 9191. (d) Choy, J.-H.; Kim, Y.-I.; Hwang, S.-J.; Yang, I.-S. *J. Solid State Chem.* **1999**, *147*, 328.

(5) (a) Rice, M. J.; Roth, W. L. *J. Solid State Chem.* **1972**, *4*, 294. (b) Armstrong, R. D.; Bulmer, R. S.; Dickinson, T. *J. Solid State Chem.* **1973**, *8*, 219.

(6) Kijima, N.; Gronsky, R.; Xiang, X.-D.; Vareka, W.-A.; Zettl, A.; Corkill, J. L.; Cohen, M. L. *Physica C* **1991**, *181*, 18.

(7) Burns, G.; Dacol, F. H.; Shafer, M. W. *Phys. Rev. B* **1977**, *16*, 1416.

(8) Mariotto, G.; Fontana, A.; Cazzanelli, E.; Fontana, M.-P. *Phys. Stat. Sol. (b)* **1980**, *101*, 341.

(9) Bottger, G.-L.; Damsgard, C.-V. *J. Chem. Phys.* **1972**, *57*, 1215.

(10) Huong, P. V.; Verma, A. L. *Phys. Rev. B* **1993**, *48*, 9869.

(11) Choy, J.-H.; Hwang, S.-J.; Kim, D.-K. *Phys. Rev. B* **1997**, *55*, 5674.

(12) Huong, P. V.; Cavagnat, R.; Verma, A. L.; Kitahama, K.; Kawai, T.; Lahaye, M.; Marquestaut, E. *J. Alloys Compd.* **1993**, *195*, 133.

(13) Muraoka, Y.; Ohnish, N.; Nagoshi, M.; Morioka, Y.; Kikuchi, M.; Hiraga, K.; Kobayashi, N.; Syono, Y. *Physica C* **1996**, *263*, 193.

(14) Ladd, M. F. C.; Palmer, R. A. *Structural Determination by X-ray Crystallography*; Plenum: New York, 1985; pp 270−273.

(15) Choy, J.-H.; Yoon, J.-B.; Kim, D.-K.; Hwang, S.-H. *Inorg. Chem.* **1995**, *34*, 6524.

(16) Turbandt, C.; Lorenz, E. *Z. Phys. Chem.* **1913**, *87*, 513.

(17) (a) Owens, B. B.; Argue, G. R. *Science* **1967**, *157*, 308. (b) Geller, S. *Science* **1967**, *157*, 310.

(18) Wittingham, M. S.; Huggins, R. A. *J. Chem. Phys.* **1971**, *54*, 414.

(19) Lehfeldt, W. *Z. Phys.* **1933**, *85*, 717.

(20) Strickler, D. W.; Carlson, W. G. *J. Am. Ceram. Soc.* **1965**, *48*, 286.

(21) Qui, D. T.; Capponi, J. J.; Gondrand, M.; Saib, M.; Joubert, J. C. *Solid State Ionics* **1981**, *3/4*, 219.

(22) In the former case ($T_d \rightarrow T_d'$), the Ag^+ ion moves toward the center of an edge of a tetrahedron, getting farther from two iodides and closer to two others, whereas in the latter ($T_d \rightarrow O_h$), it gets closer to three iodides and farther from one.

(23) Yvon, K.; Francois, M. *Z. Phys. B: Condens. Matter* **1989**, *76*, 413−444.

(24) In the case of IBi2212, the host block should move by half a unit cell in the [110] direction to maximize the chemical interaction with the symmetric iodine layer, whereas the staggered configuration of Bi2212 remains unchanged upon Ag−I intercalation, since this conformation is more effective in interacting with an asymmetric silver iodide sublattice.

(25) Kakihana, M.; Osada, M.; Käll, M.; Börjesson, L.; Mazaki, H.; Yasuoka, H.; Yashima, M.; Yoshimura, M. *Phys. Rev. B* **1996**, *53*, 11796.

(26) Denisov, V.-N.; Mavrin, B.-N.; Podobedov, V.-B.; Alexandrov, I.-V.; Bykov, A.-B.; Goncharov, A.-F.; Mel′nikov, O.-K.; Romanova, N.-I. *Solid State Commun.* **1989**, *70*, 885.

(27) Sapriel, J.; Schneck, J.; Scott, J.-F.; Toledano, J.-C.; Pierre, L.; Chavibnon, J.; Daduet, C.; Chaminade, J.-P.; Boyer, H. *Phys. Rev. B* **1991**, *43*, 6259.

(28) Liu, R.; Klein, M.-V.; Han, P.-D.; Payne, D.-A. *Phys. Rev. B* **1992**, *45*, 7392.

(29) Huong, P. V.; Pires, A.; Tomasini, S.; Wang, H.; Marguestant, E. *Physica C* **1994**, *235−240*, 497.